Dynamics of sleep oscillations is coupled to brain temperature on multiple scales

M. Csernai[1]†, S. Borbély[1]†, K. Kocsis[1,2]†, D. Burka[1], Z. Fekete[3,4], V. Balogh[1], Sz. Káli[5], Zs. Emri[6],
P. Barthó[1*]

[1]Sleep Oscillations Res. Group, RCNS, Hungarian Acad. of Sci., Budapest, Hungary; [2] Roska Tamás Doctoral School of Sciences and Technology, Fac. of Information Technol. & Bionics, Pázmány Péter Catholic Univ., Budapest, Hungary; [3]Res. Group for Implantable Microsystems, Fac. of Information Technol. & Bionics, Pázmány Péter Catholic Univ., Budapest, Hungary; [4]Inst. of Tech. Physics & Material Sci., Centre for Energy Research, Hungarian Acad. of Sci., Budapest, Hungary; [5]IEM, Hungarian Acad. of Sci., Budapest, Hungary; [6]Eszterházy Károly Univ., Eger, Hungary, [7]Corvinus Univ. of Budapest, Budapest, Hungary; † contributed equally * correspondence to: bartho.peter@ttk.mta.hu

Abstract

Every form of neural activity depends on temperature, yet its relationship to brain rhythms is poorly understood. In this work, we examined how sleep spindles and slow oscillations are influenced by changing brain temperatures, and how brain temperature is influenced by sleep oscillations. We employed a novel thermoelectrode designed for measuring temperature while recording neural activity. We found that spindle frequency is positively, duration is negatively correlated with brain temperature, while slow oscillations were not consistently affected. Local heating of the thalamus replicated the temperature dependence of spindle parameters in the heated area only, suggesting biophysical, rather than global modulatory mechanisms, a finding also supported by a thalamic network model. Finally, we show that switches between oscillatory states also influence brain temperature on a shorter and smaller scale. Epochs of paradoxical sleep, as well as the infra-slow oscillation were associated with brain temperature fluctuations below 0.2 °C. Our results highlight that brain temperature is massively intertwined with sleep oscillations on various timescales.

Introduction

Sleep is essential for our everyday functioning, as well as for memory consolidation. Several factors influence sleep, temperature being amongst the most important. Sleep quality and propensity are highly dependent on thermal conditions, sleep regulation is tightly coupled to thermoregulation. On the other hand, there are multiple sleep-related changes in body and brain temperature independent of the circadian rhythm.

Studies in mammalian species have shown that there are multiple changes in body and brain temperature during a single sleep session. Non-REM sleep is associated with decreased brain and body temperature, while during REM sleep, despite the reduced somatic thermal regulation, brain temperature increases (Kawamura & Sawyer, 1965; Baker & Hayward, 1967; Satoh, 1968; Kovalzon, 1973; Alföldi *et al.*, 1990; Lyamin *et al.*, 2018).

Besides these short-term changes, core body temperature can vary across individuals (Sund-Levander *et al.*, 2002), with changes in ambient temperature (Alföldi *et al.*, 1990), in pathological conditions, such as hypo- or hyperthyreoidism (Fregly *et al.*, 1961), during the oestrus cycle (Driver *et al.*, 1996), or as a result of medical or recreational drug use (Kiyatkin, 2010). Furthermore, though brain temperature is widely recognized as a strictly regulated homeostatic parameter, it can change as much as 3 °C across different arousal states and during sensory stimulation as shown across many avian and mammalian species (Delgado & Hanai, 1966; McElligott & Melzack, 1967; Kovalzon, 1973; Kiyatkin *et al.*, 2002; Mitchell *et al.*, 2006; Trübel *et al.*, 2006), as well as in clinical human studies (Mellergård, 1995; Rossi, 2001).

The tight relationship between core body temperature and sleep stages was also verified by directly manipulating either of them. Changes in body temperature have the potential to entrain brain state fluctuations (Whitten *et al.*, 2009), also baseline temperature influences particular brain oscillations. A brain temperature change of 1°C is sufficient to shift EEG frequencies above 10 Hz by 1Hz (Deboer & Tobler, 1995). Lowering body temperature results in a decreasing EEG amplitude (Massopust *et al.*, 1965; Michenfelder & Milde, 1991) and a shift towards lower frequencies (Deboer & Tobler, 1995). Temperature-dependent changes in sleep oscillations which reflect the activity of synchronized neural populations, point towards deeper consequences in network function.

Amongst thalamocortical oscillations, sleep spindles (7-15 Hz, 1-3 sec) have been the subject of many studies on sleep quality, memory encoding and mental health. These transient oscillations play critical role in learning (Fogel *et al.*, 2007; Morin *et al.*, 2008) and mark sleep

fragility (Lecci *et al.*, 2017), at the same time they are very susceptible to thermal changes of the mammalian body. Thus, it is essential to study how spindle dynamics are affected by body and brain temperature variations. It has been shown that the frequency of sleep spindle oscillations co-varies with physiological body temperature changes reoccurring across the menstrual cycle. Spindle activity also shows a circadian modulation with a peak density at habitual sleep onset, time locked to the maximal decrease in core temperature (Dijk & Czeisler, 1995).

Given the large natural variability in brain temperature across individuals and conditions, it is extremely important to shed light on its relationship with sleep oscillations. Medications and external thermal conditions both alter brain temperature and should therefore be considered as a factor in medical procedures. On the other hand, brain temperature should be taken into consideration when conducting *in vivo* neurophysiological experiments, as well as for *in silico* network models, in order to mimic natural state changes.

In this study we seek to elucidate the biophysical and network mechanisms underlying the relationship between sleep oscillations and brain temperature. We investigate the changes in these oscillations, especially sleep spindles, while manipulating core as well as brain temperature, and finally we show how sleep oscillations relate to brain temperature without external manipulation.

Results

Core and brain temperature modulate sleep spindle frequency

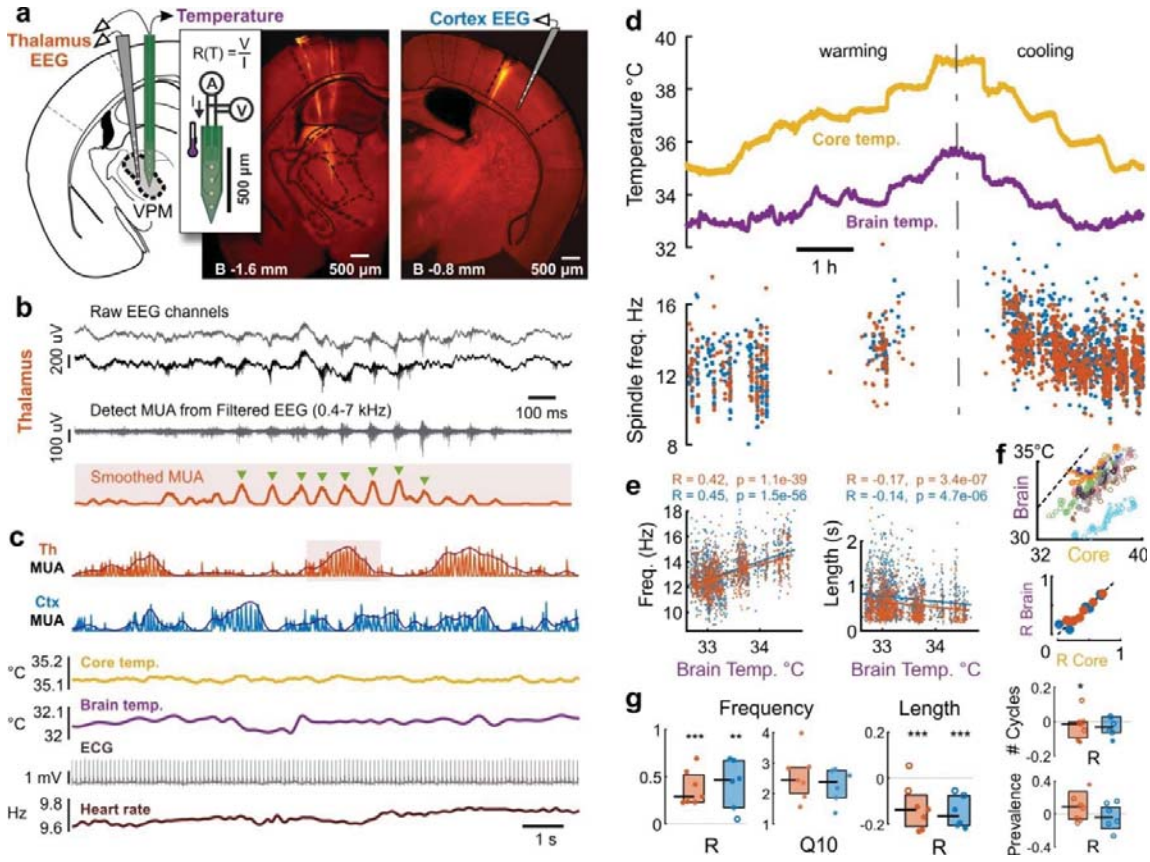

Figure 1: Sleep spindle frequency and length correlates with brain temperature.

a) Recording of LFP, MUA and temperature from VPM with linear 16 channel probe (left DiI track), and with our custom designed thermoelectrode. Temperature is measured by four-wire resistance measurement of the platinum filament in the thermoelectrode calibrated to 1mA current (inset). (right) Control LFP recordings with linear 16 channel probe from contralateral primary somatosensory cortex (shown) or VPM. **b**) Raw LFP channels are band pass filtered (gray trace), then, detected units are combined from multiple channels and smoothed with a moving average filter (smoothed MUA). The frequency of the spindle is calculated from the time between peaks (green triangles) and averaged across cycles. **c**) Sample recording chunk showing from top to bottom: thalamic raw and smoothed MUA (shaded area enlarged in (b)), cortical raw and smoothed MUA, core and brain temperature, electrocardiogram (ECG), and heart rate calculated from ECG. **d**) Example of core body and brain temperature under warming and cooling protocols. Spindle frequency is modulated by both core and brain temperature both in the thalamus and cortex. **e**) (left) Both thalamic and cortical spindle frequency correlates with brain temperature in the example shown on top. Length of the spindles has an inverse

correlation with brain temperature (right). **f**) (top) Both under warming and cooling protocols the core body temperature correlates with brain temperature across multiple animals (n=8, R=0.91, p<10-10). (bottom) Modulation of spindle frequency is consistent across core and brain temperature. **g**) (from left to right) Pooled results show that temperature dependence of spindle frequency is a significant effect (t-test, *** p<0.005, ** p<0.01, * p<0.05). Q10 value of spindle frequency perfectly fits the biological range of 2-3. Spindle length is modulated only weakly, while number of spindle cycles and spindle prevalence do not depend on brain temperature.

Our first aim was to investigate the temperature dependence of thalamocortical oscillations with no or minimal interference from global thermoregulation. To this end we employed urethane anesthesia, known to impair thermoregulatory processes (Malkinson *et al.*, 1988), yet closely mimic natural sleep (Clement *et al.*, 2008). Thus the core body temperature could be manipulated by external heating within physiological boundaries, enabling the examination of how temperature changes as large as 4-5 °C alter sleep oscillations.

Local field (LFP) and multiunit activity (MUA) was recorded from the thalamus and cortex of anesthetized mice (n=8), while the animals core body temperature was maintained between 34-39 °C. To simultaneously measure brain temperature and ongoing neural activity, we used a thermoelectrode of our own design (Fekete *et al.*, 2017). This probe has regular recording sites for unit activity, as well as a temperature sensitive meander, capable of measuring the temperature of the surrounding tissue with an absolute precision of <0.2 °C (relative precision < 0.002 °C). The thermoelectrode was placed in the primary somatosensory thalamus (VPM/VPL), while 16-channel linear silicon probes were also placed in the contralateral cortex / thalamus (Fig. 1a).

We detected sleep spindles form both thalamic and cortical MUA and calculated their frequency (Fig. 1.b and c). Besides LFP signals and brain temperature, we simultaneously recorded core temperature and electrocardiogram (see Methods) and calculated heart rate variation from the detected R-waves of the ECG signal (Fig 1.e). Fig. 1.f shows an example recording of core body and brain temperature under warming and cooling protocols we used. First, after initial surgery and the implantation of sensors, by controlling the heating pad under the mouse, we let the core temperature of the animal cool down to 35 °C. Next, in 30 minute segments, we increased the temperature of the heating pad such that the core temperature increased by ~0.5 °C in each recording segment, until the core temperature reached 39 °C. In half of the animals, the order of heating and cooling was interchanged. This assured that we collect a large number of spindles in a steady state temperature of different levels, excluding

the effect of temperature dynamics and directionality. Brain temperature closely followed changes in core temperature (Fig 1f), across all animals (Fig 1i), brain temperature being lower by 2-3 °C, as expected in small animals under anesthesia (LaManna *et al.*, 1989).

Spindle frequency was consistently modulated by both core and brain temperature, both in the thalamus and cortex (Fig 1f). We quantified this effect by calculating the correlation between brain temperature and spindle frequency. Fig 1.g illustrates this for the example above that both thalamic and cortical spindle frequency moderately correlates with brain temperature. We pooled those animals' data where the number of detected spindles exceeded 100 (thalamus: 6, cortex: 7), and these aggregate results show that the modulatory effect of temperature on spindle frequency is significant (R=0.38 +/- 0.07, t-test p=0.0017). Spindle duration was negatively correlated with temperature (Fig 1. left), while spindle prevalence (middle) and number of cycles (right) did not depend on brain temperature. The modulation of spindle frequency can be expressed as the Q10 value (the rate of change when increasing the temperature by 10 °C), and we measured a median value of 2.44 for the thalamic spindles in our pooled data (Fig. 1.i). In conclusion, frequency and duration of sleep spindles strongly depends on brain temperature.

UP/DOWN states are not correlated to thalamic temperature

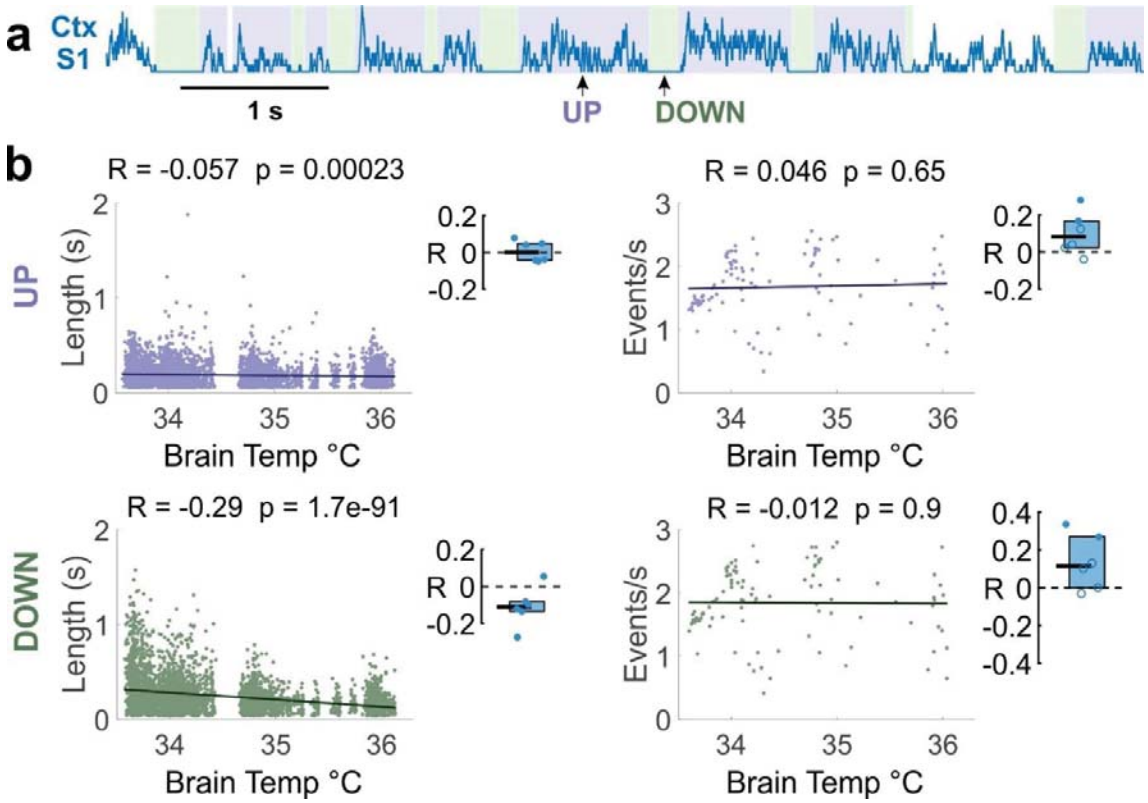

Figure 2: Characteristic slow oscillation features are not dependent on brain temperature. **a**) Up and Down states are detected from multiunit activity of somatosensory cortex. **b)** Representative examples of cortical Up (top row) and Down (bottom row) state length (left column) and prevalence (right column) correlation to brain temperature. Insets: pooled data (n=6 animals) of correlations coefficients show that slow oscillation features do not significantly depend on temperature (pooled significance is checked with t-test at 0.05 level).

Next, we were interested whether slow oscillations show similar temperature dependence. Up and down states were detected from multiunit activity in the cortex (Fig. 2a). While individual animals mainly produced significant correlations between up- and down state duration and brain temperature, the direction of these correlations varied between positive and negative values, therefore showing no significant results in the pooled data (Fig 2b, left insets). Similarly, the prevalence of Up- and Down states showed no significant dependence on brain temperature in the pooled data (Fig 2b, right insets). Overall, we found no consistent effect of temperature on slow oscillations.

Local heating increases spindle frequency locally

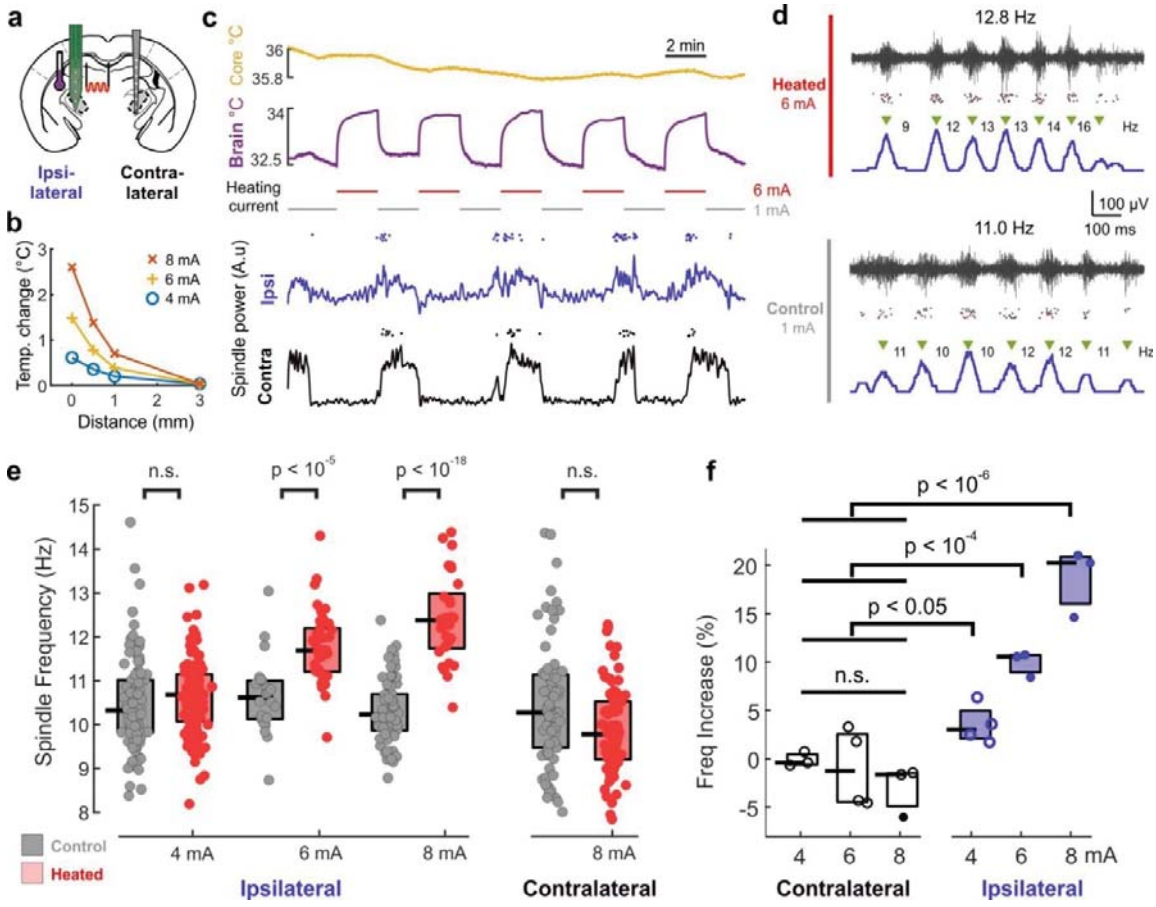

Figure 3: Temperature influences sleep spindles by a local mechanism.

a) Experimental setup: in one hemisphere, VPM/VPL thalamus was locally heated with the thermoelectrode, while neural activity was recorded both locally and in the contralateral thalamus. **b**) Tissue temperature increases due to heating of the thermoelectrode filament with different currents. Note that tissue temperature shows a sharp decay with distance from the thermoelectrode. **c**) Ipsilateral thalamus was heated in 2 min on / 2 min off cycles (top). Spindling epochs occurred irrespective of the heating cycle in both hemispheres (bottom, line: spindle power; dots: individual detected spindles). **d**) Representative examples of recorded spindles during and without heating (black trace: filtered recording, dots: detected multiunit spikes, blue line: smoothed MUA). Note that unit activity and spindle structure is undisturbed. **e**) Local heating induces significant increase in spindle frequency in case of 6 and 8 mA heating current, but no increase on the contralateral side (one-tailed two-sample t-test). **f**) Pooled results of 4 animals show a gradual effect in thalamic spindle frequencies with increasing heating current (open circles: non-significant effect, filled circles: significant effect with one-tailed two-sample t-test at p=0.01; pooled significance: two-sample t-test).

Temperature dependence of sleep spindles can arise either from biophysical mechanisms of the TC - nRT loop, or via the influence of a global, temperature sensitive modulatory system. This can be tested by locally heating the spindle-generating thalamic circuitry, with the rest of the brain and the contralateral thalamus remaining at their resting temperature. We took advantage of the fact that, besides measuring temperature, the sensor filament of our thermoelectrode is capable of heating the surrounding tissue (Fig 3a). Passing currents at, or above 4 mA, instead of the small measuring current of 1 mA, the thermoelectrode increases the local temperature in a gradual fashion up to 3 °C and this heating effect is relatively local (Fig 3b). Also, the direct current passing the probe does not stimulate the unit activity electrically (Fekete *et al.*, 2017).

In these experiments, we placed the thermoelectrode with the platinum filament in the left VPM, from where we recorded both temperature as well as LFP. The animals core temperature was kept at 36 ± 0.2 °C. We applied heating currents of 4-8 mA. Also, we placed a linear electrode in the contralateral VPM for control recording (Fig. 3.a). The heating current was applied in a cyclic protocol (2 min heating / 2 min measuring), while maintaining core temperature constant (Fig. 3.c). The heating cycles did not disrupt the periodic recurrence of spindling epochs, as they appeared simultaneously with those on the contralateral hemisphere (Fig 3.c bottom), and they did not disrupt the internal structure of the spindles (Fig 3.d).

As seen on Fig 3.e, application of three heating currents (4,6,8 mA) produced a progressive increase in local spindle frequency as compared to the control periods, while not affecting the spindles in the contralateral hemisphere. The phenomenon persists on a pooled data of 4 animals (Fig 3.f), from a small, but significant increase of spindle frequency at 4 mA to 20% increase at 8 mA. Again, there was no significant effect at the contralateral thalamus, though a controversial, non-significant spindle frequency decrease was observable at the highest heating current. Duration of the spindles also decrease significantly in case of 8 mA heating by 25.7 +/- 3.8 % ($p=0.019$). These results imply that the temperature dependence of spindle frequency is largely due to local biophysical mechanisms.

In silico TC-nRT model reproduces temperature dependence of spindle frequency

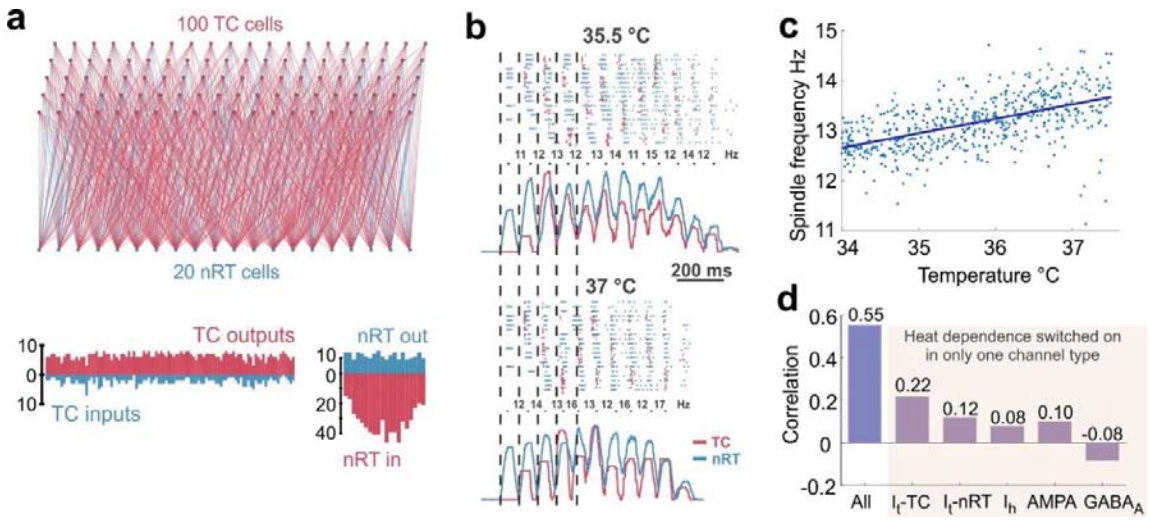

Figure 4. Network model reproduces temperature dependence of sleep spindles.

a) Schematic of the network topography (above), and the number of connections for each TC an nRT cell (below). **b**) Representative example spindles produced by the same network at two different temperatures. Top: raster plot of TC and nRT units' spiking, bottom: smoothed multiunit activity for TC and nRT cells. Note that the spindle at 37 °C is faster. **c**) Correlation between temperature and spindle frequency calculated from 500 individual spindles. **d**) Correlations from simulations where temperature dependence was switched on for the labeled currents only.

To further elucidate the possible mechanisms of the temperature dependence of sleep spindles, we created a thalamic network model consisting of single compartment TC and nRT cells. The model consisted of 100 TC and 20 nRT cells (Fig. 4.a) that were randomly connected with a loose topography and were capable of producing transient oscillations at the frequency domain of sleep spindles. Figure 4.b shows an example of spindles generated by the same network at 35.5 and 37 °C, the latter showing a higher frequency. The pooled analysis of 500 random networks (Fig 4.c) revealed a marked correlation ($R=0.55$, $p<0.001$) between spindle frequency and temperature.

To reveal whether a single current is responsible for this effect we reproduced these results with the temperature dependence turned on for each individual current only (I_t-TC, I_t-nRT, I_h, AMPA, $GABA_A$), respectively. We found that each current contributed to the effect by a small degree (Fig. 4.d), with the exception of $GABA_A$, which, when being temperature-

dependent alone, produced a small negative correlation. Thus, the model reproduced the effects of temperature change observed in mice with statistically significant correlation between the temperature and spindle frequency as a further evidence for the biophysical nature of this effect.

Infra-slow oscillations co-modulate temperature, heart rate and sleep oscillations

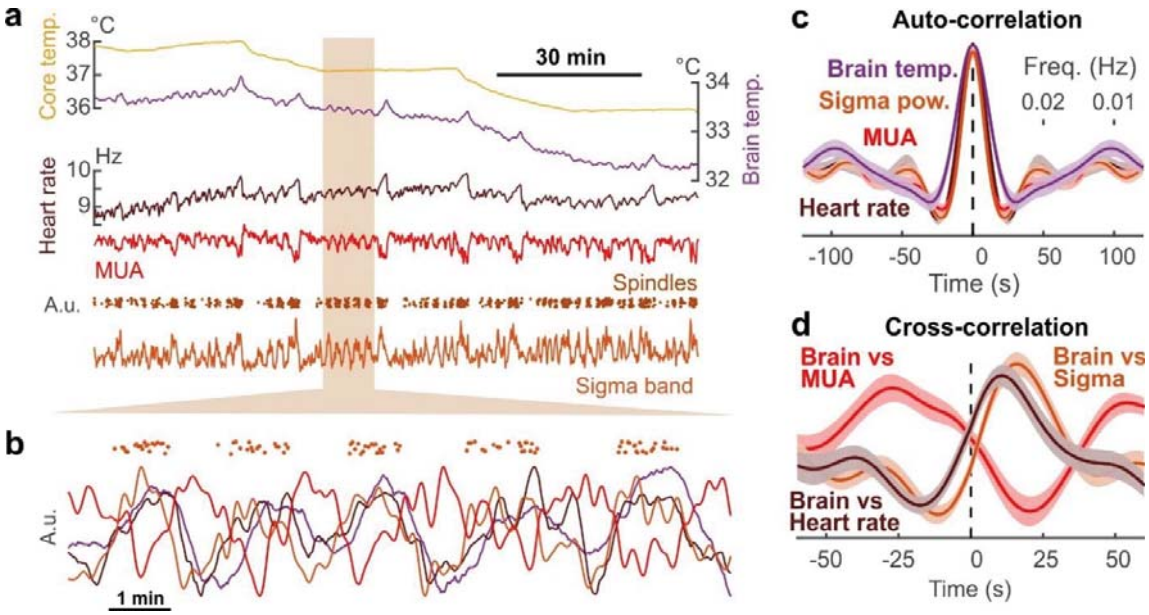

Figure 5. Microfluctuations in brain temperature accompany spindling epochs.

a) Example recording where microfluctuations of brain temperature, heart rate and spindle power appear to be in synchrony. **b**) When zooming in on a finer timescale, sigma power, heart rate and brain temperature oscillate together with an apparent temporal order between them. **c**) Averaged autocorrelograms of pooled urethane data show that these microfluctuations are in the infra-slow frequency range (~0.02 Hz). **d**) Pooled cross correlation (brain temp vs other) shows that spindling and heart rate foregoes brain temp fluctuation, while general multiunit activity (MUA) lags behind.

So far we have analyzed the temperature dependence of sleep oscillations during external manipulation. Here we were interested in the microarchitecture of brain temperature variations under natural conditions, and the effects of these changes on sleep oscillations.

Detailed inspection of the temperature traces under urethane revealed that besides the gross changes induced by heating and cooling, brain temperature also shows periodic

fluctuations on a scale smaller by an order of magnitude (Fig 5.a). These fluctuations were superimposed on, and appeared irrespectively of the absolute brain temperature. Based on their amplitude and frequency, two types of fluctuations were differentiated.

Type I. fluctuations were larger (0.22 +/- 0.014 °C from baseline to peak), and reoccurred on a ~10 minute timescale (more details are provided in Table 1). Type II. fluctuations were smaller (0.019 +/- 0.0008 °C from trough to peak), occurred with 0.022 Hz frequency, interposed between cycles of Type I. fluctuations. Under urethane anesthesia, both types of fluctuations were associated with individual spindle events, increase in sigma power, and elevation of heart rate (Fig 5.b). The periodicity of Type II. fluctuations (Fig 5.c) corresponded to the frequency of infra-slow oscillation (Lecci *et al.*, 2017) and there is a clear temporal order between them (Fig 5.d).

Next, we were interested whether these temperature fluctuations also exist during natural sleep. Animals were chronically implanted with miniature NTC thermistors in the thalamus (see methods), as well as tungsten electrodes to monitor cortical and thalamic LFP and multiunit activity, electromyogram and heart rate (Fig 6.a). Both Type I. and Type II. fluctuations were observed in naturally sleeping animals (Fig 6.bc).

During natural sleep, Type I. fluctuations appeared slightly more frequently than under urethane (0.021 +/- 0.0002), and with a smaller amplitude (0.012 +/- 0.0002 °C). They coincided with a surge in the theta-delta ratio of hippocampal activity (Fig. 6.b), the hallmark of REM sleep. We analyzed how changes in sleep oscillations, muscle activity and heart rate correlated in time relative to the peak of these large temperature fluctuations (Fig. 6.c shows pooled results). In general, broadband multiunit activity closely followed these elevations (16.5 +/- 6.6 s median peak delay). As expected, hippocampal LFP theta-delta ratio activity was closely correlated, preluding these large temperature fluctuations by 8.8 +/- 5.4 s. In contrast to urethane anesthesia, sigma power and spindling preceded Type I. elevations by a relatively large median time of 49.4 +/- 9.6 s. We also calculated the time lags of these parameters at half amplitude, and these metrics confirm the temporal order described above. Note that neck muscle activity increases as both temperature as well as theta power declines, which is probably due to microarousals often following REM epochs. We may also see a slight increase in the averaged heart rate during these events, but this seems to be a negligible effect due to the large dispersion of the heart rate peaks relative to the respective temperature peaks.

Type II. fluctuations under natural sleep occurred interspersed between Type I. elevations, with similar parameters as in urethane anesthetized animals (0.012 +/- 0.0002 °C

from trough to peak, mean period length 47.9 +/- 0.5 s). Their amplitude was smaller than under urethane, though this is likely to be a measurement effect; the NTC thermistor integrating signal from a larger area, therefore being less sensitive to local changes in temperature than the thermoelectrode. Type II. fluctuations appeared in synchrony with thalamic multiunit activity, sigma power and individual spindles, as well as heart rate variation. Fig 6.e and g shows the autocorrelograms of the example epoch and the average of all epochs, respectively. On both autocorrelograms, there is a marked first peak in the 0.02 Hz range, corresponding to the period of infra-slow oscillation. Moreover, we found that the temporal order between these signals during these small fluctuation epochs is constrained. Broadband multiunit activity closely follows the temperature fluctuations (-0.65 +/- 0.8 s delay), sigma power lags behind (7.5 +/- 0.8 s delay) while heart rate variation preludes it (-11.92 +/- 0.9 s delay), as it is shown on the cross correlations on Fig 6.f (example epoch) and h (pooled results). Note that the cross correlation of sigma power and heart rate shows inverse relation (Fig 6.h inset), which is in concordance with earlier results (Lecci *et al.*, 2017). In summary, both REM epochs and infra-slow oscillation are accompanied by changes in brain temperature, irrespective of the baseline temperature.

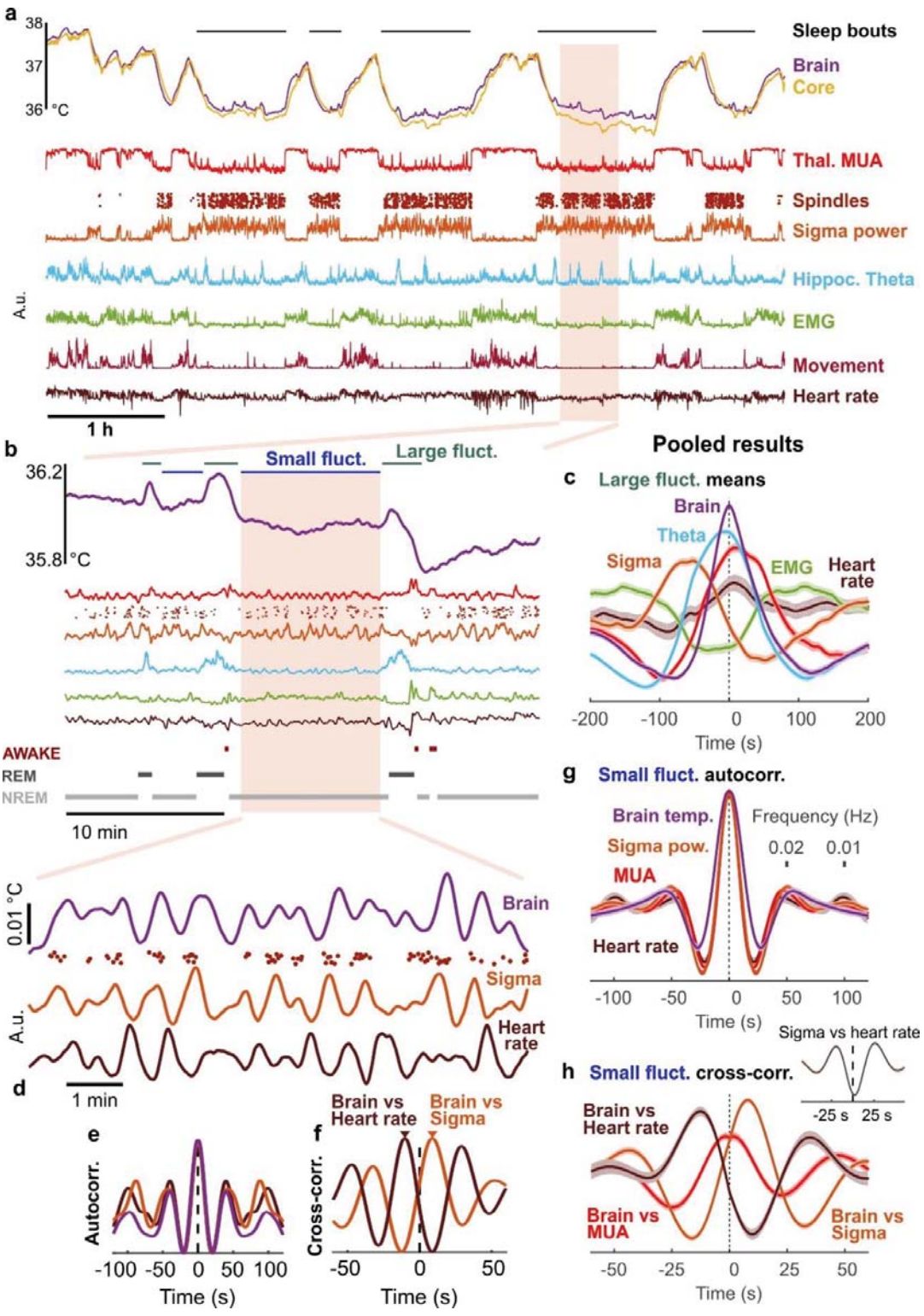

Figure 6. Spontaneous infra-slow microfluctuations of physiological signals in natural sleep.

a) Example recording during wakefulness and sleep showing core and brain temperature, neural activity, locomotion/EMG and heart rate. **b**) The microarchitecture of sleep becomes apparent

in a sleep bout, and we may differentiate between epochs of large and small fluctuations in brain temperature. **c**) Pooled results show that the large temperature fluctuations provide a constrained frame to the fluctuations of other physiological signals. **d**) Example of a small fluctuation epoch. **e-f**) Autocorrelograms of the traces above show that these microfluctuations are in the infra-slow frequency range (~0.02 Hz). **g-h**) Cross correlations show that spindling foregoes temperature spikes, heart rate variation follows them, while broadband multiunit activity is in sync with the temperature.

	Natural sleep	**Urethane anesthesia**
Number of animals	3	3
Total recording time	52.2 hours	14.6 hours
% of sleep	69%	-
Number of sleep bouts	42	-
Avg. length of sleep bout	50.6 5 +/- 3.6 min	-
Large fluctuations (Type I.)		
- Number of fluctuations	141	19
- Num. of fluct. in a sleep bout	3.92 +/- 0.3	-
- Amplitude	0.15 +/- 0.005 °C	0.22 +/- 0.014 °C
- Length	117.8 +/- 3.8 s	155.2 +/- 12.8 s
- Period length	639.3 +/- 36 s	963.1 +/- 119 s
Small fluctuations (Type II.)		
- Number of fluct. epochs	133	22
- Length of fluct. epochs	484.7 +/- 21.7 s	667.7 +/- 88.6 s
- Num. of fluct. epochs in a bout	3.69 +/- 0.4	-
- Num. of fluct. cycles	1237	309
- Cycle amplitude	0.012 +/- 0.0002 °C	0.019 +/- 0.0008 °C
- Cycle period length	47.9 +/- 0.5 s	44.8 +/- 1.1 s
- Num. of cycles in an epoch	9.1 +/- 0.5	14 +/- 2

Table 1.: Parameters of infra-slow temperature fluctuations in natural sleep and under urethane anesthesia.

Discussion

To study the relationship of sleep oscillations and temperature we recorded thalamic and cortical neural activity with simultaneous measurement of core body and brain temperature. We found that the frequency of sleep spindles correlates with brain temperature, most likely originating from biophysical properties of local circuits, instead of global modulatory mechanisms. We also show that during natural sleep brain temperature is modulated by the infra-slow oscillation, as spindling and REM epochs are associated with microfluctuations in brain temperature. Our results suggest that thalamocortical oscillations and brain temperature influence each other during physiological, as well as pathological states.

Previous studies

Though temperature dependence of EEG rhythms have been described before, to our knowledge this is the first study to systematically combine LFP and multiunit recordings with brain temperature measurements, as well as use local heating and computational modeling to explain the underlying mechanism. (Hoagland, 1936) described higher frequency alpha-rhythms in patients undergoing hyperpyretic treatment, decreases in barbiturate-spindle frequency was found during cooling in cats (Andersen *et al.*, 1967), and similar results were found in infants during surgical hypothermia (Schmitt *et al.*, 2002). Also, (De Vera *et al.*, 1994) *examined EEG activity in Gallotia galloti* lizards and found that the frequency of spindle-like activity increases with body temperature, though these oscillations produce a continuum from 2-30Hz, marking them as a different rhythm from mammalian spindles. A robust decrease in all EEG frequencies, especially theta has been found in hibernating Djungarian hamsters (Deboer & Tobler, 1995; Deboer, 1998). Our results are generally in line with these results, as the frequency of spindle oscillations showed a positive correlation with temperature. In the case of slower rhythms, (Sheroziya & Timofeev, 2015) showed that local cortical cooling eliminates slow oscillations, giving way to desynchronized activity. Here we did not find consistent temperature effect on slow oscillations, though this may be due to the methodological differences between the two studies. Is in the Sherozya paper they considered relatively short term (below 10s) changes, whereas in our study the examined periods were 30 minutes long. Also local cortical cooling effects the thalamus only indirectly, while global temperature modulation influences the whole thalamocortical system.

Technical considerations

In the first part of this study, we used urethane anesthesia to abolish thermoregulatory processes, so that we could manipulate the experimental animal's temperature freely. Question is, can we apply these results to unanesthetized subjects? Urethane anesthesia is considered a good model of natural sleep (Clement *et al.*, 2008; Pagliardini *et al.*, 2013), as it produces most sleep EEG rhythms with minor differences. Sleep spindles under urethane are very similar to those in natural sleep, except for their more limited spatial synchrony (Barthó *et al.*, 2014). Also, as we show here, the 0.02 Hz periodic alternation between epochs of high sigma and high delta power, the so called infra-slow oscillation (Lecci *et al.*, 2017) occurs both under urethane and natural sleep, with the same frequency. Finally, urethane anesthetized animals produce REM-like epochs with characteristic hippocampal theta oscillations, though these have a lower frequency (3-5 Hz) than during real REM (6-8 Hz), and are sensitive to atropine administration (Kramis *et al.*, 1975).

A seemingly surprising phenomenon in our data is that the brain temperature is consistently below the core body temperature in all anesthetized recordings. In fact, this is a well-known phenomenon. Awake animals, and large animals under anesthesia, have a positive brain-body temperature gradient (Hamilton, 1963; Hayward & Baker, 1969; Mitchell *et al.*, 2006; Hebert *et al.*, 2008). Small animals under anesthesia, on the other hand, have a negative brain-body temperature gradient, (Serota & Gerard, 1938; McElligott & Melzack, 1967; LaManna *et al.*, 1989) most likely due to the higher brain-surface ratio, and the impaired thermoregulation due to the anesthetic. Nevertheless, we show that the brain can produce sleep oscillations at 2-3 °C below physiological brain temperature, therefore we can accept urethane anesthesia as a suitable tool for our experiments.

Temperature dependence of biological processes

It is well-known that temperature has an effect on the rate of biological processes (van't Hoff, 1884; Arrhenius, 1889), with a temperature coefficient (Q10) between 2 and 3, so that the speed of the process doubles or triples as temperature increases by 10°C (Demirhan *et al.*, 2010). Despite a constantly redistributed cerebral heat, neuronal activity is a function of temperature, physiological and pathological temperature changes of the brain can be derived from the changes of local metabolism, cerebral blood perfusion, and blood temperature (Hayward & Baker, 1969). Brain cells show a Q10 of 2.3 (Michenfelder & Milde, 1991) or

even higher in the physiological temperature range. Temperature dependence of electrophysiological properties in the neuron is well defined. Passive membrane properties, resting potential, action potential generation, ionic transport, conduction velocity, synaptic transmission and neurotransmitter reuptake are all dependent on thermal conditions (B Katz, 1965; Brooks, 1983; Thompson *et al.*, 1985; Volgushev *et al.*, 2000; Tryba & Ramirez, 2004; Lee *et al.*, 2005). Cerebral metabolic rate and oxygen-affinity of hemoglobin are also affected by temperature change (Guyton & Hall, 2005). The sum of these effects may dramatically change neuronal network activity. Temperature dependence of neural oscillations is usually also described by the Q10 value, which is 2.3- 2.7 for neural oscillations (Deboer & Tobler, 1995). Our results show a Q10 of ~2.5 in case of sleep spindles, suggesting that this value may be a general phenomenon in the nervous system. It is worthy to note that several poikilothermic animals, such as certain crustaceans and mollusks , employ compensatory mechanisms to make their neural oscillators robust to temperature changes (Partridge & Connor, 1978; Tang *et al.*, 2012). Whether a similar mechanism exists in the mammalian thalamocortical system remains to be elucidated.

Global vs. local regulation

The main thermoregulatory center in the brain is the Preoptic Area (POA) of the hypothalamus. POA receives input from peripheral thermoreceptors, but also contains intrinsically heat-sensitive neurons that are hypothesized to monitor changes in brain temperature. The same region contains neurons that project to several modulatory centers (Peterfi *et al.*, 2009), involved in sleep maintenance. POA contains warm-sensing neurons, known to be activate during sleep (Alam *et al.*, 1996). Therefore, it wouldn't be surprising if body temperature influenced sleep rhythms via the posterior hypothalamus. Though it is unclear whether POA can directly influence brain thermoregulation, if it does, it may influence the level of neuromodulators in the process, therefore influencing neural oscillations. Our results suggest that this is not the case, as local heating of the thalamus alters spindles ipsi- but not contralaterally. There is a possibility that locally heating the thalamus also warms the hypothalamic POA to a certain degree. Indeed, Figure 3. shows that while local heating increases spindle frequency on the ipsilateral side, there is a smaller, non-significant adverse effect on the contralateral side that might arise from increased hypothalamic temperature perception, but this effect is smaller by a magnitude than that of local thalamic heating.

Brain temperature changes accompany state changes

Besides brain temperature influencing neural oscillations, spontaneous changes of brain states may alter brain temperature in one way or another. We found that both REM, and on a smaller scale, spindling epochs are associated with elevated brain temperature.

Although the body's temperature regulation switches off during REM (Parmeggiani, 1977), paradoxically, brain temperature increases, as has been described in rabbit (Kawamura & Sawyer, 1965), cat (Satoh, 1968), rat (Kovalzon, 1973; Obál *et al.*, 1985), and even fur seal (Lyamin *et al.*, 2018) (though some monkey studies reported just the opposite (Reite & Pegram, 1968; Hayward & Baker, 1969)). It is debated, whether this effect is aimed to protect brain function from REM-associated hypothermia, or simply reflects the increased metabolic activity due to increased unit firing.

Spindling epochs in the rodent are periods resembling human stage II. sleep, recurring with a periodicity of 0.02 Hz. This infra-slow oscillation has been observed in both rodents and humans (Steriade *et al.*, 1993; Lecci *et al.*, 2017), modulating EEG sigma band as well as heart rate (Lecci *et al.*, 2017), pupil size (Blasiak *et al.*, 2013), and fMRI BOLD signal (Mantini *et al.*, 2007). We found that brain temperature fluctuates in synchrony with the infra-slow oscillation, including sigma power, individual spindle events, as well as heart rate. What can be the cause of these fluctuations? Physiological and pathological temperature changes of the brain can be directly derived from the changes of local metabolism, cerebral blood perfusion, and blood temperature (Hayward & Baker, 1969; Wang *et al.*, 2014). In our case, the temperature elevations were correlated with increased multiunit activity, which may increase temperature directly, or via enhancing the local blood flow.

Significance of brain rhythm alterations

What is the significance of temperature induced changes in brain rhythms? Though their exact function is still debated, the general consensus is that sleep oscillations play a major role in learning and memory consolidation. Several studies reported increases in slow wave and spindle activity during sleep after learning tasks (Feld & Born, 2017). Also, transcranial DC stimulation (Marshall, 2004), or phase-locked auditory stimulation (Ngo *et al.*, 2013) of slow waves during sleep can enhance consolidation of declarative memories. Aside from learning, spindle duration and frequency is affected in a variety of pathological states, including

schizophrenia (Manoach *et al.*, 2016). Spindle duration and frequency also correlates with intelligence (Bódizs *et al.*, 2014).

As learning involves both long-term potentiation (LTP) and long-term depression (LTD) of synapses, packets of synchronized neural activity, such as up-states or cycles of sleep spindles make these oscillations an ideal candidate for 'burning in' new memories. The frequency range of sleep spindles is especially suited for inducing LTP in cortical circuits (Rosanova & Ulrich, 2005). A change in the frequency of this oscillation is likely to affect synaptic potentiation in one way or another. Indeed, a 2°C drop in body temperature markedly reduces information recall (Coleshaw *et al.*, 1983). Another aspect of thalamocortical oscillations is the binding hypothesis (Nikolić *et al.*, 2013), stating that oscillations create a temporal window for selected groups of neurons to fire together to form a representation. Though originally proposed for gamma oscillations in awake subjects, it is probable that spindles operate along the same logic in a different scenario, in which case, frequency matters.

Our data show that body along with brain temperature changes have an important but underrated role in sleep quality. Since pharmaceutics and other medical or experimental interventions can alter brain temperature, leading to spindle frequency changes as high as 2-3 Hz, they need to be taken into consideration for the planning and analysis of both animal research and medical procedures.

Materials and Methods

Ethical Considerations

Experiments were carried out in accordance with the Hungarian Act of Animal Care and Experimentation (1998, XXVIII) and with the directive 2010/63/EU of the European Parliament and of the Council of 22 September 2010 on the protection of animals used for scientific purposes. Experimental protocol was approved by the regional ethical committee (license number PEI/001/2290-11/2015 for our in vivo experiments). Efforts were made to minimize the number of animals used.

Mice were kept under a 12:12 h LD cycle (lights-on at 7:00 a.m.) in a temperature-controlled room at 22±2 °C. Standard food-pellets and tap water were available *ad libitum*.

Electrophysiological and temperature recordings

Acute experiments. Our experiments were performed on 13 male C57BL/6 mice (Toxicoop, Budapest, Hungary) weighing between 18 and 30 g at the time of the surgery. The animals were anesthetized with urethane (1 g/kg; i.p.), then placed in a stereotaxic instrument (RWD Life Science; Shenzhen, China).

To record local field potential (LFP) activity, NeuroNexus (Ann Arbor, USA) silicon probes were inserted into the brain. Linear 16-channel silicon probes were inserted to the left primary somatosensory cortex (Br. AP 0.0, L +3.5, in 18º at 1600 μm depth), and in the left ventral posteromedial nucleus (VPM) of thalamus (Br. AP -1.6, L +2.3, in 18º at 3700 μm depth). Our custom designed thermoelectrode, featuring four electrophysiological recording sites and a platinum temperature sensor, was inserted also to the left VPM (Br. AP -1.6, L +1.6, in 0º at 3600 μm depth). In some experiments the linear 16-channel probe was inserted to the right primary somatosensory cortex (Br. AP 0.0, L -3.5, in 18º at 1600 μm depth) or to the right VPM (Br. AP -1.6, L -2.3, in 18º at 3700 μm depth). In this case there was no recording from left cortical area. An additional screw electrode implanted over the cerebellum served as a reference. Coordinates are based on the stereotaxic atlas of Paxinos and Watson (1986). Using unipolar V_1 ECG lead heart rate and electrocardiogram was simultaneously recorded with LFP. Rectal temperature was measured by a TH-5 Thermalert Monitoring Thermometer (Physitemp; Clifton, USA).

Recordings were made with Intan RHD2132 16-channel amplifiers, connected to an RHD-2000 Evaluation Board. Brain temperature was measured by calibrating and measuring the resistance of the platinum filament in the thermoelectrode (see details in (Fekete *et al.*, 2017)) by a Keithley 6221 precision current generator and a Keithley 2000MM multimeter (Keithley Instruments Inc, OH, USA). Rectal temperature signals were simultaneously recorded by using the analog inputs of the Intan RHD-2000 system. All signals were sampled at 20 kHz, except for brain temperature, which was sampled at 5 Hz and synchronized to the other signals through the analog input of the Intan system.

Chronic experiments. These experiments were carried out on 5 male C57BL6 mice (Toxicoop, Budapest, Hungary) weighing between 27 and 35 g at the time of the surgery. For initial surgery, animals were anesthetized with ketamine/xylazine (ketamine: 100 mg/kg; xylazine: 4 mg/kg; i.p.), then placed in a stereotaxic instrument (RWD Life Science; Shenzhen, China).

To record LFP and multiuint (MUA) activity, bundles of 25 and 50 µm tungsten stereotrodes (California Fine Wire; Grover Beach, USA) were used. Electrodes were placed in the left and right S1 (Br. AP 0.0, L ±3.5, at 1000 µm depth), the ventral posteromedial thalamus (VPM) (Br. AP -1.6, L +2.5, in 18º at 3700 µm depth), in as well as the hippocampus (Br. AP -1.6, L -1.5, in 0º at 2200 µm depth). To record temperature, a 0.3 mm diameter Semitec thermistor (223Fµ3122-07U015, Mouser Electronics; Mansfield, USA) was also inserted to left VPM (Br. AP -1.6, L +1.5, in 0º at 3600 µm depth). An EMG electrode was placed in neck musculature. Coordinates are based on the stereotaxic atlas of Paxinos and Watson (1986). Electrodes were connected to a Neuralynx EIB-16 electrode interface board (Neuralynx, Dublin, Ireland). Core body temperature was measured intraperitoneally by Semitec thermistors (223Fµ3122-07U015, Mouser Electronics; Mansfield, USA).

After at least 10 days of recovery, signals were recorded continuously for 6-8 hours / day during wakefulness and natural sleep with the same system as acute experiments. The behavior of animals was also recorded using a commercially available CCD camera.

Histology

Following the recordings, under deep anesthesia mice were transcardially perfused with 0.9% saline, followed by fixative containing 4% paraformaldehyde and 0.1M phosphate buffer (PB). After perfusion brains were sliced to 50µm thick coronal sections with a vibratome. Before each acute experiment, silicon probes were dipped in DiI solution for verification of

recording sites. After further PB washes, sections were mounted temporarily in PB and imaged using epifluorescent microscopy (Leica).

The electrode tracks of the thermo probes were reconstructed from counterstained glial fibrillary acidic protein (GFAP). GFAP staining were used to visualize the lesion made by the thermo probes and to check whether heating caused necrosis in the adjacent tissue. After imaging silicon probe tracks, the same sections were subjected to immunofluorescence staining according to the following protocol. After further PB washes, sections were freeze-thawed above liquid N_2 in 0.1M PB containing 30% sucrose. Endogenous peroxidase activity was blocked with 1% H_2O_2, then non-specific staining was suppressed with 2% Normal Horse Serum (NHS, Vector Laboratories, Burlingame, CA, USA) in 0.1M PB. Monoclonal mouse antibodies were used against GFAP (1:2000, EMD Millipore, clone GA5) for 24h at 4ºC. Immunopositive elements were visualized using biotinylated anti-mouse immunoglobulin G (1:250, Vector Laboratories, Burlingame, CA, USA) as a secondary antiserum followed by avidin-biotinylated horseradish peroxidase complex (ABC; 1:250, Vector Laboratories, Burlingame, CA, USA). The immunoperoxidase reaction was developed using 3,3'-diaminobenzidine tetrahydrochloride (DAB; Sigma, St Louis, MO, USA) dissolved in Tris buffer (TB, pH 7.6) as a chromogen. After washing in Tris buffer and PB, sections were mounted, dehydrated for light microscopy (2x10min in xylene) and coverslipped with DePex (Serva Electrophoresis GmbH, Heidelberg, Germany). We found no necrosis in any of the animals.

Local heating of brain tissue

The platinum filament in the thermoelectrode can be used to heat up neighboring brain tissue by increasing the current in the 4-wire resistance measurement setup. The technical and histological details are described in (Fekete *et al.*, 2017). Briefly, we employed 2 minutes of measurement current (1 mA) and 2 minutes of heating current (4-8 mA) in a cyclic pattern. An exponential was fitted on the measured temperature values from 400 ms after the offset of the heating current in each cycle and temperature during heating was estimated by the intersection of the exponential and the offset time of the heating pulse.

Data analysis

Electrophysiology. Raw LFP channels were band pass filtered between 0.4-7 kHz, and multiunits were detected with an absolute threshold. The units were combined from multiple channels, downsampled to 1 kHz and smoothed with a 10 ms moving average filter. Sigma power was determined by filtering the preprocessed multiunit activity (MUA) between 6-18 Hz. In case of the analysis of infra-slow oscillations we used sigma power from best recording sites. Theta power was calculated by first downsampling hippocampal LFP to 1 kHz, and then taking the ratio of the theta (6-10 Hz) and delta (0.5-4 Hz) bands.

Temperature. In general, all temperature data was downsampled to 1kHz and smoothed with 100ms window, except for brain temperature in the acute experiments, in which case we simply used the recorded samples that were synchronized to the other signals. In case of the analysis of infra-slow oscillations, all respective signals were smoothed with a 10s window and then downsampled to 10 Hz, while brain temperature of the acute experiments were interpolated to 10 Hz. Large fluctuations were marked manually based on visual features of joint brain temperature and theta power increase motifs. Small fluctuation epochs were selected between the large elevations. Small fluctuation cycle peaks and troughs were detected automatically by the findpeaks MATLAB function, and we manually validated these detected peaks in each epoch.

Spindle detection and frequency calculation. Spindles were detected semi-automatically from the MUA (for details, see (Barthó *et al.*, 2014)). After automatic detection, spindles were verified visually, in some cases, added manually, and false detections were deleted. Frequency of the spindle was calculated from the average of time difference between automatically detected cycle peaks (Fig 1.b). The temperature of the spindle is defined as the temperature at the start of the respective spindle.

Detection of UP and DOWN states. UP states are detected from slow wave sleep epochs by first smoothing MUA signal with 80 ms window, next, taking an absolute threshold on the signal, then collecting epochs that are consecutively over the threshold, which are longer than 40 ms and have activity level under the threshold (‘silence’) for at least 40 ms before and after them. DOWN states are simply detected which are under the threshold for at least 40 ms.

Model

For the purpose of this study we adapted the network model of thalamocortical (TC) and thalamic reticular (nRT) cells, constructed by Destexhe et al (Destexhe *et al.*, 1994, 1996) in the NEURON modeling environment. Single compartment TC and nRT cell membrane potential was governed by the following equations:

$$\boldsymbol{C_m\dot{V}_{TC} = -g_L(V_{TC} - E_L) - I_{KL} - I_T - I_h - I_{Na} - I_K - I_{GABA_A}} \quad (1)$$

$$\boldsymbol{C_m\dot{V}_{nRT} = -g_L(V_{nRT} - E_L) - I_{T2} - I_{CAN} - I_{AHP} - I_{Na} - I_K - I_{AMPA}} \quad (2)$$

where V_{TC} and V_{nRT} are the membrane potentials of TC and nRT cells respectively, while $C_m = 1\ \mu F/cm^2$ is the membrane specific capacity. The first part of each equation is the leak current, in which g_L is the leak membrane potential and E_L is the reversal potential of the leakage. In case of the TC cells the leak potassium current (I_{KL}) is implemented separately from the other leakage. I_T and I_{T2} are low threshold calcium currents, where the second is a slower version used in the nRT cells. I_h is the hyperpolarization activated cation current of the TC cells. The nRT cells also include a calcium activated nonselective cation current (I_{CAN}) and slow calcium dependent potassium current (I_{AHP}) (Destexhe *et al.*, 1994). I_{Na} and I_K are sodium and potassium currents that generate action potentials based on the Hodgkin-Huxley model. I_{GABA_A} is the current of the GABA-A receptors that appear in the synapses from nRT to TC cells, and I_{AMPA} is the current of the AMPA receptors from the TC to nRT synapses.

TC cells activated nRT cells via AMPA receptors while nRT cells inhibited TC cells via GABA-A receptors. We disregarded GABA-B receptors since their blockade hardly altered spindle oscillations experimentally (Krosigk *et al.*, 1993; Bal *et al.*, 1995). Synaptic currents were based on the models constructed by Destexhe et al (Destexhe *et al.*, 1996) supplemented with temperature dependency. Both currents can be described by the following equations:

$$I_{syn} = \bar{g}_{syn} r\big(V - E_{syn}\big) \quad (3)$$

$$\frac{dr}{dt} = \alpha[C](1 - r) - \beta r \quad (4)$$

where syn can be substituted for AMPA or GABA-A, and I_{syn} is the synaptic current, $\bar{g}_{syn}$ is the maximal conductance and E_{syn} is the reversal potential, respectively. The fraction of open channels is denoted by r and $[C]$ is the concentration of neurotransmitters in the synaptic cleft, while α and β are the forward and backward binding rates of neurotransmitters for the given receptor type. We also define the following variables:

$$\tau_r = \frac{1}{\alpha C_{max} + \beta} \quad (5)$$

$$r_\infty = \frac{\alpha C_{max}}{\alpha C_{max} + \beta} \quad (6)$$

$$\boldsymbol{\varphi_h = Q_{10}^{\frac{T - T_{exp}}{10^\circ C}}} \quad (7)$$

where τ_r is the time constant of channel binding, r_∞ is the steady-state fraction of open channels and φ_h is the temperature dependent multiplier that was added to the original model. C_{max} is the maximum concentration of transmitters, T is the actual temperature and T_{exp} is the experimental temperature the binding rates were measured at. The temperature coefficients (Q_{10}) of AMPA and GABA-A receptors were estimated based on the work of Postlethwaite et al. (Postlethwaite *et al.*, 2007) and Otis and Mody (Otis & Mody, 1992), respectively.

An analytical expression exists for the fraction of open receptors based on the phase of the transmitter release, which is approximated with a simple pulse:

$$\boldsymbol{r = r_\infty + (r - r_\infty) \exp\left(-\frac{\varphi_h \Delta t}{\tau_r}\right)} \text{ if the pulse is on} \quad (8)$$

$$\boldsymbol{r = r \exp(-\varphi_h \beta \Delta t)} \text{ if the pulse is off} \quad (9)$$

For further details on the deduction of these equations refer to the original model.

Conductances were adjusted to reproduce spindle oscillation with the characteristics described by Barthó et al (Barthó *et al.*, 2014). Model cells matched the firing patterns of both TC and nRT cells, and spindles generated by the model reproduced waxing and waning behavior but were slightly longer than the measured counterparts. Our computer codes of the model are available online at https://github.com/BarthoLab/SpindleTemperatureModel.

Model topography

For the construction of the model we interpret the connections of the network as a bipartite directional graph where the two sets of nodes are the TC and nRT cells. We used a 1-dimensional network: both sets of cells are on a one unit long line with equal distances between them, and the two lines of the two sets are parallel to each other. For the sake of reproducibility we used a deterministic random number generator based on the Mersenne Twister algorithm (MATLAB 2016a) to choose target cells. Our examined networks consisted of 100 TC cells and 20 nRT cells. Each TC cell targets 8 different nRT cells from the closest 20, based on normal distribution. The nRT cells target 20 different TCs from the closest 50. We did not allow

reciprocal connections in our networks. The algorithm creates the network without any consideration of the reciprocal rule, and it trims these pairs after the completion of the structure. In the case of bidirectional TC and nRT connections, one is removed based on a coin flip.

The strength of a given synaptic connection in the network is given by the weight associated with it. Connection weights are normally distributed with a mean as the default synaptic strength. This approach makes it theoretically possible to create topologically analogous networks that have completely different behaviors because of the different synapses. We created over 10 thousand different networks – where the topology was based on different random seeds – and ran them for 2s on random temperatures between 34.0 C and 37.5 C.

Spindle detection methods were similar to the ones used in real life measurements. Low spindle frequency was a sign of detection failure in most of the manually examined results, thus we automatically excluded cases with a spindle frequency lower than 8Hz from our analysis.

Statistical Analysis

Parametric statistical tests were used based on normality of observed distributions tested with Kolmogorov-Smirnov test at 0.05 significance level. In all statistical tests with no significant results, power of the tests were above 0.75 with sample sizes used in the study, based on minimal effect size of 0.2 in case of correlation comparisons and 1 Hz for spindle frequency difference. Throughout the paper we show mean values +/- standard error of mean (SEM), unless specified otherwise. All analysis was done in MATLAB (Mathworks).

Acknowledgments

This work was supported by Hungarian Scientific Research Fund OTKA K119650, PD121307, National Brain Research Program 2017_1.2.1-NKP-2017-00002 and Bolyai Research Scholarship of the Hungarian Academy of Sciences

References

Alam MN, McGinty D & Szymusiak R (1996). Preoptic/anterior hypothalamic neurons: Thermosensitivity in wakefulness and non rapid eye movement sleep. *Brain Res* **718,** 76–82.

Alföldi P, Rubicsek G, Cserni G & Obál F (1990). Brain and core temperatures and peripheral vasomotion during sleep and wakefulness at various ambient temperatures in the rat. *Pflugers Arch* **417,** 336–341.

Andersen P, Andersson SA & Lomo T (1967). Some factors involved in the thalamic control of spontaneous barbiturate spindles. *J Physiol* **192,** 257–281.

Arrhenius S (1889). On the Reaction Velocity of the Inversion of Cane Sugar by Acids. *Zeitschrift für Phys Chemie*226–248.

B Katz RM (1965). The effect of temperature on the synaptic delay at the neuromuscular junction. *J Physiol* **181,** 656.

Baker MA & Hayward JN (1967). Autonomic Basis for the Rise in Brain Temperature during Paradoxical Sleep. *Science (80-)* **157,** 1586–1588.

Bal T, von Krosigk M & McCormick DA (1995). Role of the ferret perigeniculate nucleus in the generation of synchronized oscillations in vitro. *J Physiol* **483,** 665–685.

Barthó P, Slézia A, Mátyás F, Faradzs-Zade L, Ulbert I, Harris KD & Acsády L (2014). Ongoing network state controls the length of sleep spindles via inhibitory activity. *Neuron* **82,** 1367–1379.

Blasiak T, Zawadzki A & Lewandowski MH (2013). Infra-Slow Oscillation (ISO) of the Pupil Size of Urethane-Anaesthetised Rats ed. Dickson CT. *PLoS One* **8,** e62430.

Bódizs R, Gombos F, Ujma PP & Kovács I (2014). Sleep spindling and fluid intelligence across adolescent development: sex matters. *Front Hum Neurosci* **8,** 952.

Brooks VB (1983). Study of brain function by local, reversible cooling. **95,** 1–109.

Clement EA, Richard A, Thwaites M, Ailon J, Peters S & Dickson CT (2008). Cyclic and sleep-like spontaneous alternations of brain state under urethane anaesthesia. *PLoS One*;

DOI: 10.1371/journal.pone.0002004.

Coleshaw SR, Van Someren RN, Wolff AH, Davis HM & Keatinge WR (1983). Impaired memory registration and speed of reasoning caused by low body temperature. *J Appl Physiol* **55,** 27–31.

Deboer T (1998). Brain temperature dependent changes in the electroencephalogram power spectrum of humans and animals. *J Sleep Res* **7,** 254–262.

Deboer T & Tobler I (1995). Temperature dependence of EEG frequencies during natural hypothermia. *Brain Res* **670,** 153–156.

Delgado JM & Hanai T (1966). Intracerebral temperatures in free-moving cats. *Am J Physiol* **211,** 755–769.

Demirhan A, Kaymaz M, AhIska R & Güler I (2010). A survey on application of quantitative methods on analysis of brain parameters changing with temperature. *J Med Syst* **34,** 1059–1071.

Destexhe A, Bal T, McCormick DA & Sejnowski TJ (1996). Ionic mechanisms underlying synchronized oscillations and propagating waves in a model of ferret thalamic slices. *J Neurophysiol* **76,** 2049–2070.

Destexhe A, Contreras D, Sejnowski TJ & Steriade M (1994). A model of spindle rhythmicity in the isolated thalamic reticular nucleus. *J Neurophysiol* **72,** 803–818.

Dijk DJ & Czeisler C a (1995). Contribution of the circadian pacemaker and the sleep homeostat to sleep propensity, sleep structure, electroencephalographic slow waves, and sleep spindle activity in humans. *J Neurosci* **15,** 3526–3538.

Driver HS, Dijk DJ, Werth E, Biedermann K & Borbely AA (1996). Sleep and the sleep electroencephalogram across the menstrual cycle in young healthy women. *J Clin Endocrinol Metab* **81,** 728–735.

Fekete Z, Csernai M, Kocsis K, Horváth ÁC, Pongrácz A & Barthó P (2017). Simultaneous in vivo recording of local brain temperature and electrophysiological signals with a novel neural probe. *J Neural Eng* **14,** 034001.

Feld GB & Born J (2017). Sculpting memory during sleep: concurrent consolidation and

forgetting. *Curr Opin Neurobiol* **44,** 20–27.

Fogel SM, Smith CT & Cote KA (2007). Dissociable learning-dependent changes in REM and non-REM sleep in declarative and procedural memory systems. *Behav Brain Res* **180,** 48–61.

Fregly MJ, Iampietro PF & Otis AB (1961). Effect of hypothyroidism on heat production and loss during acute exposure to cold. *J Appl Physiol* **16,** 127–132.

Guyton A & Hall J (2005). *Textbook of Medical Physiology*, 11th edn. Saunders.

Hamilton CL (1963). Hypothalamic temperature records of a monkey. *Proc Soc Exp Biol Med* **112,** 55–57.

Hayward J & Baker M (1969). A comparative study of the role of the cerebral arterial blood in the regulation of brain temperature in five mammals. *Brain Res* **16,** 417–440.

Hebert J, Lust A, Fuller A, Maloney SK, Mitchell D & Mitchell G (2008). Thermoregulation in pronghorn antelope (Antilocapra americana, Ord) in winter. *J Exp Biol* **211,** 749–756.

Hoagland H (1936). Temperature Characteristics of the "Berger Rhythm" in Man. *Science (80-)* **83,** 84–85.

Kawamura H & Sawyer CH (1965). Elevation in brain temperature during paradoxical sleep. *Science* **150,** 912–913.

Kiyatkin E a (2010). Brain temperature homeostasis: physiological fluctuations and pathological shifts. *Front Biosci* **15,** 73–92.

Kiyatkin EA, Brown PL & Wise RA (2002). Brain temperature fluctuation: A reflection of functional neural activation. *Eur J Neurosci* **16,** 164–168.

Kovalzon VM (1973). Brain temperature variations during natural sleep and arousal in white rats. *Physiol Behav* **10,** 667–670.

Kramis R, Vanderwolf CH & Bland BH (1975). Two types of hippocampal rhythmical slow activity in both the rabbit and the rat: relations to behavior and effects of atropine, diethyl ether, urethane, and pentobarbital. *Exp Neurol* **49,** 58–85.

Krosigk M Von, Bal T & Mccormick DA (1993). Cellular Mechanisms of a Synchronized

Oscillation in the Thalamus. *Science (80-)* **261,** 361–364.

LaManna JC, McCracken KA, Patil M & Prohaska OJ (1989). Stimulus-activated changes in brain tissue temperature in the anesthetized rat. *Metab Brain Dis* **4,** 225–237.

Lecci S, Fernandez LMJ, Weber FD, Cardis R, Chatton J-Y, Born J & Lüthi A (2017). Coordinated infraslow neural and cardiac oscillations mark fragility and offline periods in mammalian sleep. *Sci Adv* **3,** e1602026.

Lee JCF, Callaway JC & Foehring RC (2005). Effects of Temperature on Calcium Transients and Ca 2+ -Dependent Afterhyperpolarizaions in Neocortical Pyramidal Neurons. *J Neurophysiol* **93,** 2012–2020.

Lyamin OI, Kosenko PO, Korneva SM, Vyssotski AL, Mukhametov LM & Siegel JM (2018). Fur Seals Suppress REM Sleep for Very Long Periods without Subsequent Rebound. *Curr Biol*1–6.

Malkinson TJ, Cooper KE & Veale WL (1988). Physiological changes during thermoregulation and fever in urethan-anesthetized rats. *Am J Physiol Integr Comp Physiol* **255,** R73–R81.

Manoach DS, Pan JQ, Purcell SM & Stickgold R (2016). Reduced Sleep Spindles in Schizophrenia: A Treatable Endophenotype That Links Risk Genes to Impaired Cognition? *Biol Psychiatry* **80,** 599–608.

Mantini D, Perrucci MG, Del Gratta C, Romani GL & Corbetta M (2007). Electrophysiological signatures of resting state networks in the human brain. *Proc Natl Acad Sci* **104,** 13170–13175.

Marshall L (2004). Transcranial Direct Current Stimulation during Sleep Improves Declarative Memory. *J Neurosci* **24,** 9985–9992.

Massopust LC, Wolin LR & Meder J (1965). Spontaneous electrical activity of the brain in hibernators and nonhibernators during hypothermia. *Exp Neurol* **12,** 25–32.

McElligott JG & Melzack R (1967). Localized Thermal Changes Evoked in the Brain by Visual and Auditory Stimulation. *Exp Neurol* **17,** 293–312.

Mellergård P (1995). Intracerebral temperature in neurosurgical patients: intracerebral

temperature gradients and relationships to consciousness level. *Surg Neurol* **43,** 91–95.

Michenfelder JD & Milde JH (1991). The relationship among canine brain temperature, metabolism, and function during hypothermia. *Anesthesiology* **75,** 130–136.

Mitchell G, Fuller A, Maloney SK, Rump N & Mitchell D (2006). Guttural pouches, brain temperature and exercise in horses. *Biol Lett* **2,** 475–477.

Morin A, Doyon J, Dostie V, Barakat M, Hadj Tahar A, Korman M, Benali H, Karni A, Ungerleider LG & Carrier J (2008). Motor sequence learning increases sleep spindles and fast frequencies in post-training sleep. *Sleep* **31,** 1149–1156.

Ngo HV V, Martinetz T, Born J & Mölle M (2013). Auditory closed-loop stimulation of the sleep slow oscillation enhances memory. *Neuron* **78,** 545–553.

Nikolić D, Fries P & Singer W (2013). Gamma oscillations: precise temporal coordination without a metronome. *Trends Cogn Sci* **17,** 54–55.

Obál F, Rubicsek G, Alföldi P & Sáry G (1985). Changes in the brain and core temperatures in relation to the various arousal states in rats in the light and dark periods of the day. *Pflügers Arch Eur J Physiol* **404,** 73–79.

Otis TS & Mody I (1992). Modulation of decay kinetics and frequency of GABAA receptor-mediated spontaneous inhibitory postsynaptic currents in hippocampal neurons. *Neuroscience* **49,** 13–32.

Pagliardini S, Gosgnach S & Dickson CT (2013). Spontaneous Sleep-Like Brain State Alternations and Breathing Characteristics in Urethane Anesthetized Mice ed. Foffani G. *PLoS One* **8,** e70411.

Parmeggiani PL (1977). Thermoregulation during sleep. *Riv Neurol* **47,** 485–491.

Partridge LD & Connor JA (1978). A mechanism for minimizing temperature effects on repetitive firing frequency. *Am J Physiol* **234,** C155-61.

Peterfi Z, Makara GB, Obál F & Krueger JM (2009). The anterolateral projections of the medial basal hypothalamus affect sleep. *Am J Physiol Integr Comp Physiol* **296,** R1228–R1238.

Postlethwaite M, Hennig MH, Steinert JR, Graham BP & Forsythe ID (2007). Acceleration of

AMPA receptor kinetics underlies temperature-dependent changes in synaptic strength at the rat calyx of Held. *J Physiol* **579,** 69–84.

Reite ML & Pegram G V (1968). Cortical temperature during paradoxical sleep in the monkey. *Electroencephalogr Clin Neurophysiol* **25,** 36–41.

Rosanova M & Ulrich D (2005). Pattern-specific associative long-term potentiation induced by a sleep spindle-related spike train. *J Neurosci* **25,** 9398–9405.

Rossi S (2001). Brain temperature, body core temperature, and intracranial pressure in acute cerebral damage. *J Neurol Neurosurg Psychiatry* **71,** 448–454.

Satoh T (1968). Brain temperature of the cat during sleep. *Arch Ital Biol* **106,** 73–82.

Schmitt B, Jenni OG, Bauersfeld U, Schüpbach R & Schmid ER (2002). Spindle activity in children during cardiac surgery and hypothermic cardiopulmonary bypass. *J Clin Neurophysiol* **19,** 547–552.

Serota HM & Gerard RW (1938). Localized thermal changes in the cat's brain. *J Neurophysiol* **1,** 115–124.

Sheroziya M & Timofeev I (2015). Moderate Cortical Cooling Eliminates Thalamocortical Silent States during Slow Oscillation. *J Neurosci* **35,** 13006–13019.

Steriade M, McCormick DA & Sejnowski TJ (1993). Thalamocortical oscillations in the sleeping and aroused brain. *Science* **262,** 679–685.

Sund-Levander M, Forsberg C & Wahren LK (2002). Normal oral, rectal, tympanic and axillary body temperature in adult men and women: a systematic literature review. *Scand J Caring Sci* **16,** 122–128.

Tang LS, Taylor AL, Rinberg A & Marder E (2012). Robustness of a Rhythmic Circuit to Short- and Long-Term Temperature Changes. *J Neurosci* **32,** 10075–10085.

Thompson SM, Masukawa LM & Prince DA (1985). Temperature dependence of intrinsic membrane properties and synaptic potentials in hippocampal CA1 neurons in vitro. *J Neurosci* **5,** 817–824.

Trübel HK, Sacolick LI & Hyder F (2006). Regional Temperature Changes in the Brain during Somatosensory Stimulation. *J Cereb Blood Flow Metab* **26,** 68–78.

Tryba AK & Ramirez J-M (2004). Hyperthermia modulates respiratory pacemaker bursting properties. *J Neurophysiol* **92,** 2844–2852.

van't Hoff MJH (1884). Etudes de dynamique chimique. *Recl des Trav Chim des Pays-Bas* **3,** 333–336.

De Vera L, González J & Rial R V. (1994). Reptilian waking EEG: slow waves, spindles and evoked potentials. *Electroencephalogr Clin Neurophysiol* **90,** 298–303.

Volgushev M, Vidyasagar TR, Chistiakova M & Eysel UT (2000). Synaptic transmission in the neocortex during reversible cooling. *Neuroscience* **98,** 9–22.

Wang H, Wang B, Normoyle KP, Jackson K, Spitler K, Sharrock M, Miller CM, Best C, Llano D & Du R (2014). Brain temperature and its fundamental properties: A review for clinical neuroscientists. *Front Neurosci* **8,** 1–17.

Whitten T a, Martz LJ, Guico A, Gervais N & Dickson CT (2009). Heat synch: inter- and independence of body-temperature fluctuations and brain-state alternations in urethane-anesthetized rats. *J Neurophysiol* **102,** 1647–1656.